ELSEVIER

Polymer 44 (2003) 2481–2491

polymer

www.elsevier.com/locate/polymer

A micro-indentation method for probing the craze-initiation stress in glassy polymers

H.G.H. van Melick[a], O.F.J.T. Bressers[a], J.M.J. den Toonder[b], L.E. Govaert[a,*], H.E.H. Meijer[a]

[a]*Dutch Polymer Institute (DPI), Section Materials Technology (MaTe), Eindhoven University of Technology, P.O. Box 513, NL-5600MB, Eindhoven, The Netherlands*

[b]*Philips Research Laboratories, Prof. Holstlaan 4, NL-5656AA, Eindhoven, The Netherlands*

Abstract

Initiation of a localised plastic zone is numerically simulated using a constitutive model that incorporates an accurate description of the post-yield behaviour with the important phenomena of strain softening and strain hardening. Subsequent nucleation of voids in the deformation zone is detected using a hydrostatic stress criterion. This criterion is identified and validated. A micro-indenter with a sapphire sphere is used to produce indents that are later examined with an optical microscope. These observations lead to a critical force at which crazes are initiated in polystyrene. Combining these experiments with a numerical study shows that the loading part of indentation can be accurately predicted. A critical hydrostatic stress of 40 MPa is extracted from the numerical model by monitoring of the local stress field at the moment that the indentation force reaches the experimentally determined force level at which crazes were found to initiate. This criterion is validated by indentations on samples with different thermal histories, and at various loading rates. Finally, the influence of network density on the value of the hydrostatic stress criterion is investigated by indentation of blends of polystyrene and poly(2,6-dimethyl-1,4-phenylene-oxide). It is shown that the critical hydrostatic stress increases with network density.

Keywords: Crazing initiation; Network density; Glassy polymers

1. Introduction

Macroscopic brittle fracture of glassy polymers is generally preceded by formation of crazes, small crack-like defects, of which the opposite faces are bridged by super-drawn fibrils. Crazes have, due to these fibrils, unlike real cracks, some load-bearing capacity and when viewed on a microscopic level, they display large plastic deformations. For this reason, crazes are the most important source of fracture toughness in brittle glassy polymers, even though the material volume involved in the deformation is generally small. It is, therefore, not surprising that a vast amount of research has been performed in the past on all aspects of crazing: craze nucleation, growth and failure, the micro-structure of crazes, the influence of molecular parameters, etc., and a number of excellent reviews are available [1–4].

Fig. 1 depicts some of the microscopic events that are likely to be involved in craze nucleation [2]. First, plastic deformation occurs at a local stress concentration. The non-linear nature of the yield process and the strain softening character of polymer glasses result in localisation of deformation as plastic strain increases. Since the material at some distance of the local deformation zone is relatively undeformed, the differences in volumetric strain induce a build-up of tri-axial stresses. At this stage two possibilities exist. Typically for (unnotched) polycarbonate, the strain-hardening response of the material can stabilise the strain-localisation process and the micro-shear band spreads out. It has been shown [5] that the hydrostatic stress required to plastically expand a micro-porous region is greatly reduced if the material is in a state of flow. The initiation of the dilatation process is enhanced by the more severe localisation, as found in (unnotched) polystyrene (and also in notched polycarbonate), since the dilative stresses become so large that void nucleation occurs and, finally, crazes develop in the deformation zone.

From this sequence of events, it is clear that the macroscopic failure behaviour of glassy polymers is determined by two factors: (1) the intrinsic post-yield behaviour of the material, and (2) its resistance against void-nucleation.

The post-yield behaviour of glassy polymers is

* Corresponding author. Tel.: +31-40-2472838; fax: +31-40-2447355.
E-mail address: l.e.govaert@tue.nl (L.E. Govaert).

0032-3861/03/$ - see front matter © 2003 Elsevier Science Ltd. All rights reserved.
doi:10.1016/S0032-3861(03)00110-1

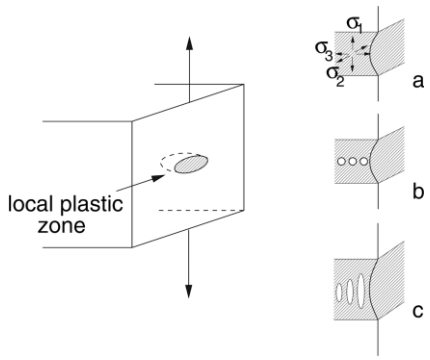

Fig. 1. Schematic drawing of microscopic events involved in craze nucleation: (a) formation of a localised surface plastic zone and build-up of lateral stresses, (b) nucleation of voids in the plastic zone and (c) deformation of the polymer ligaments between voids and coalescence of individual voids to form a void network (after [2]).

characterised by strain softening and strain hardening [6] and, although the exact molecular origin of strain softening is still largely unknown, it is well documented that strain softening exhibits a pronounced dependence on the thermal and mechanical history [6–13]. Slow-cooling rates tend to increase strain softening, whereas quenching leads to moderate or, in case of polyvinylchloride (PVC), even negligible softening [7]. The phenomenon appears to be related to the erasure of physical ageing effects by plastic deformation: mechanical rejuvenation. The origin of strain hardening is well established: a contribution of the entanglement network as a result of stress-induced segmental mobility [6,12,14].

The extent to which polymers are susceptible to strain localisation is determined by a subtle interplay between strain hardening and strain softening [15]. The initiation of localised deformation zones is governed by strain softening, which allows the zone to grow with decreasing stress, elastically unloading its surrounding. The amount of strain hardening determines whether or not the deformation zone is stabilised [15–17]. Strain softening, however, appears to be the key factor in this localisation phenomenon. Upon removal, or strong reduction, of strain softening through thermal (quenching) or mechanical (plastic pre-deformation) methods, the occurrence of strain localisation is inhibited. Prime examples are homogeneous deformation of quenched PVC [7] and remarkable transition from crazing to macroscopic plastic flow in polystyrene after a mechanical treatment consisting of a thickness reduction of 30% by means of rolling [13]. These effects are, however, of a temporary nature, as strain softening tends to return in time as a result of physical ageing [13,15].

In the past 15 years, considerable effort was directed towards the numerical simulation of strain localisation phenomena. The development of 3D constitutive models that were able to capture the post-yield behaviour of glassy polymers started off with the work of Boyce and co-workers at MIT [18–21]. This work was later followed by studies of the group of van der Giessen [22,23] and our group [11,12,24–30]. As a result of these activities the numerical simulation of plastic localisation in various loading geometries is now well established.

Also substantial research effort has been conducted in the identification of craze initiation criteria for amorphous polymers. Narisawa and co-workers investigated a range of amorphous polymers, mostly in notched tensile and bending tests, and determined values for critical dilative stresses [31–33]. However, considering the defect sensitivity and, consequently, initiation of crazes at the surface, such a test is inappropriate for polystyrene. This was recognised by Camwell and Hull [34], who compressed a polystyrene sheet between flat dies, during which both shear bands and crazes were generated in the same specimen. Narisawa et al. [32] slightly modified this experiment into a plane-strain indentation between parallel plates using a flat-punch. Using Hill's slip-field line theory, they derived a critical hydrostatic stress of around 25 MPa for polystyrene, although the validity of their approach was questioned by Kells and Mills [35] in a similar approach. The adequate description of the small and large strain deformation behaviour of glassy polymers by using the compressible Leonov model, enabled us, in a combined experimental and numerical study, to monitor the stress/strain fields in this plane-strain indentation test, that indeed included large local plastic deformation [36]. Despite the elegance of the indentation technique to generate a craze in the bulk (rather than at the surface) of the material in a reproducible way, two major drawbacks were encountered. First, the size of the specimens ($60 \times 20 \times 6$ mm^3) resulted in some uncertainty about the exact thermodynamical state of the material and makes a clear distinction between quenched and annealed material virtually impossible. Hence the exact intrinsic properties which are required in the finite element analysis cannot be determined. Second, a clear influence of friction and lubrication between the supporting plates, providing the plane strain conditions, was observed at the high indentation loads (≈ 9 kN). The stress fields in the experiments most probably will not be equal to these corresponding to the true plane strain conditions in the simulations. Most striking in this respect is the inability to capture the force-displacement curve in a quantitative way, for which the numerical model had already proven its capability in compression, tension and, in a more complex geometry, spherical indentation tests [11,12,37]. In an axi-symmetric set-up the friction problems could be solved but, due to the larger sample size, more problems would arise concerning the thermodynamical state of the material.

In conclusion, an experiment is required that circumvents the defect-sensitivity of polystyrene, that allows for thin samples with a well-defined thermal and mechanical history and that can be described accurately by finite element simulations. As a spin-off from a previous project [37], indentation with spherical indenters on flat polymeric surfaces has proven to be an accurate experiment to generate crazes in a well-controlled and reproducible way.

At a certain load during indentation, pile-up of material occurs next to the contact area between indenter and polymer. Besides plastic deformation, positive hydrostatic stresses evolve in this pile-up which results in small crazes just below the surface of the polymer. To identify the local stress distribution within the pile-up, finite element simulations of the indentation experiment can be performed. As a material model, the compressible Leonov-model [11, 24,25] is used, which captures the complex yield behaviour of glassy polymers quite well. The capability of this model to describe the indentation of amorphous polymers was already shown [37]. The hydrostatic stress criterion is obtained by a combination of numerical simulations and experimental observations. From the experiments the force is recorded at which crazes are initiated. Using a numerical simulation the critical hydrostatic stress is identified as the maximum hydrostatic stress in the pile-up zone at this specific indentation force.

The applicability of the criterion obtained is subsequently investigated by comparing numerical predictions of craze initiation with experimental observations at various loading rates (i.e. indentation force rates) and on samples with different thermal histories (quenched and annealed PS). Using the same approach the influence of network density on the critical hydrostatic stress is studied by indentation of blends of polystyrene and poly(2,6-dimethyl-1,4-phenylene-oxide) (PPO).

2. Materials and experimental methods

2.1. Materials

The base materials used were commercial polystyrene (Styron 634, Dow Chemical) and two blends of polystyrene (PS) and poly(2,6-dimethyl-1,4-phenylene-oxide) (PPO 803, General Electric Plastic), that contained, respectively, 20 and 40% PPO. The granular material was compression moulded into plates of $100 \times 100 \times 3\ mm^3$ in a stepwise manner. In the middle of the mould a thin glass-plate was placed to obtain a smooth surface, suitable for indentation.

The material was pre-heated in the mould at 90 °C above its glass-transition temperature (T_g) for 15 min and then compressed in 5 min, at the same temperature, in 5 steps of increasing force (up to 300 kN). In between these steps, pressure was released to allow for degassing. The mould was then placed into a cold press and cooled to room temperature at a moderate force (100 kN).

From the centre of these plates small square platelets were cut ($20 \times 20\ mm^2$). In order to eliminate residual stresses and thermal history effects the platelets were heat-treated for 30 min at 15 °C above T_g. Subsequently, the platelets were given a thermal treatment, either annealing or quenching. During annealing the samples were held at 20 °C below T_g for three days and, subsequently, slowly cooled in one day in an oven to room temperature. During quenching the samples were cooled rapidly in ice-water from 15 °C above T_g.

2.2. Experimental setup

Indentations were performed on a micro-indenter; a custom-designed apparatus at Philips Research Laboratories in Eindhoven. The forces that can be measured range from 20 mN up to 20 N with an accuracy of 2 mN; the accuracy of the displacement is 20 nm. Forces and displacements were measured by means of coils at the bottom of the indenter column. The indenter used was a sapphire sphere, with a radius of 150 μm, glued onto a brass holder. The compliance of the apparatus was determined by a reference measurement on silica glass. The elastic indentation depth-force curve was predicted by Hertz' theory. From the deviation between the theoretical and experimental curve, the compliance was determined to be $6 \times 10^{-2}\ \mu mN^{-1}$, and the corresponding stiffness of the measuring system is $1.67 \times 10^7\ Nm^{-1}$.

A typical indentation procedure starts with a position-controlled movement of the indenter towards the sample until the surface is contacted, with a pre-load of 5 mN. Next the platelet is loaded, in force control, up to a predefined maximum force at force rates ranging from 10 mNs^{-1} up to 1 Ns^{-1}. When a predefined maximum force is reached, the indenter is retracted in position control. The retraction velocity is adjusted to the loading rate to keep the time of loading and unloading identical. During indentation both the load and the displacement are recorded. The experiments are performed in a sequence of increasing force steps. At each step of 0.5 N, the indentations are repeated at least 10 times. After the experiments, the indents are examined using an optical microscope (Leica DM/RM) to check whether crazes were formed at the force applied. This microscope uses polarised light for the Interference-contrast to visualise the crazes.

To obtain the material parameters, required for the numerical simulations, uniaxial compression tests were performed on a servo hydraulic MTS Elastomer Testing System 810. Cylindrical specimens (∅ 6 mm × 6 mm) were compressed at room temperature and a constant logarithmic strain rate between two parallel, flat steel plates. The friction between the sample and the steel plates was reduced using PTFE tape (3M 5480, PTFE skived film tape) on the sample and a soap–water mixture on the surface between the steel and the tape. No bulging or buckling of the sample was observed, indicating that the friction was sufficiently reduced. A constant true logarithmic strain rate varying from 10^{-4} up to $10^{-2}\ s^{-1}$ was achieved in strain control.

2.3. Numerical methods

To obtain a quantitative criterion for craze nucleation, numerical simulations of the indentation experiment were carried out. Information that could not be extracted from the

experiments, such as stresses and strains in the indented material, was derived from the model. By comparing the computed forces and displacements with the experimental results, the numerical model was validated. From the experiments a critical force for craze initiation was determined and from the accompanying simulations a quantitative craze-nucleation criterion was derived.

2.3.1. Material model

Numerical simulations are only useful if the intrinsic deformation behaviour is covered well. In previous work, an elasto-viscoplastic constitutive equation for polymer glasses was introduced, the so-called compressible Leonov-model, of which the relevant equations are briefly summarised in the appendix. The nomenclature and meaning of the material parameters used in this study can be found in [11,24,25].

2.3.2. FEM model

Two deformable bodies are considered: the indenter and the material examined. The contact between indenter and sample is assumed to be frictionless (the influence was examined by varying the friction in the model and was found to be negligible). In the axi-symmetric model, the polystyrene sample chosen is large enough to prevent the edges influencing the stress-distribution, and the sapphire indenter is modelled as a half-sphere (see Fig. 2a). The z-axis is the axis of rotational symmetry.

Axi-symmetric conditions require the nodes positioned on the z-axis to be fixed in radial direction. Furthermore, rigid-body movement of the sample is prevented by fixation on the right-hand side. The deformable indenter, which can only be moved in z-direction, is loaded on the left-hand side and pressed into the sample at a constant, pre-defined loading rate.

The materials used in the numerical simulations were sapphire (indenter) and polystyrene. The sapphire was assumed to be linear elastic and properties were taken from literature ($E = 304$ GPa and $\nu = 0.234$ [38]), whereas the parameters of the polystyrene were extracted from uni-axial compression tests, represented in Fig. 3.

To exclude any mesh-dependence a stepwise element refinement was performed until the solution converged to a steady, mesh independent, result. In order to prevent excessive computation times the mesh refinement was restricted to areas of interest (see Fig. 2b).

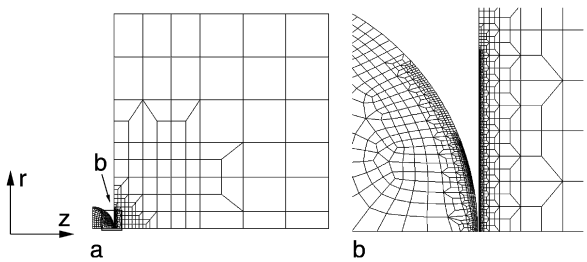

Fig. 2. Finite element mesh used in simulations: (a) indenter (left) and sample, (b) zoomed region with mesh-refinement.

3. Results

3.1. Materials characterisation

3.1.1. Bulk properties

Material parameters required for the numerical simulations are extracted from uni-axial compression tests at room temperature. In this loading geometry localisation of deformation is inhibited and the true stress/true strain behaviour can be obtained up to large (compressive) strains. Fig. 3 shows the rate dependence of PS at strain rates ranging from 3×10^{-4} up to $3 \times 10^{-3}\ s^{-1}$, representative for the strain rates occurring during indentation.

The strain rate predominantly influences the level of the yield stress and has a less pronounced influence on the post-yield behaviour: strain softening and strain hardening. The continuous lines in Fig. 3 are predictions using the compressible Leonov-model with the parameters indicated in Table 1. From the yield stresses, obtained at various strain rates, the model parameters A and τ_0 can be determined. The softening parameters D_∞ and h are fitted on the compression curve at $1 \times 10^{-3}\ s^{-1}$, whereas the strain hardening modulus is defined as the slope of the curve at large strains of the true-stress versus $\lambda^2 - \lambda^{-1}$ (neo-Hookean behaviour). For the Young's modulus E and the Poisson ratio ν, literature values are taken [39].

The one-mode model used here assumes linear elastic behaviour up to the yield point, and as a result the strain at yield is slightly under-predicted. Since, in reality, the pre-yield behaviour is (non-linear) visco-elastic, the model can be expected to be less satisfactory in predicting the behaviour in the unloading part of the indentation. A multi-mode version of the model performs much better, see e.g. [25], but requires too much computational time for the problem under consideration. Moreover, an accurate description of the loading curve proves to be more relevant for this investigation than that of the unloading curve. The

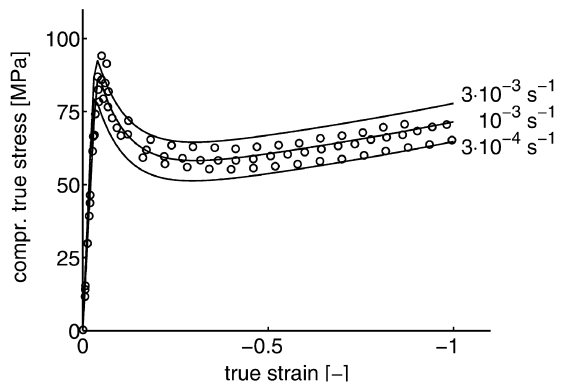

Fig. 3. Rate-dependent compressive behaviour of polystyrene, experiments (circles) and simulations (continuous lines).

Table 1
Material parameters for all materials, derived from uniaxial compression tests, used as input for the numerical simulations

Material	E (MPa)	A (s)	τ_0 (MPa)	h (−)	D_∞ (−)	G_R (MPa)
PS, quenched	3300	2.6×10^8	2.56	40	7	11
PS annealed	3300	1.0×10^{12}	2.56	75	11	11
PS/PPO 80/20	3000	1.0×10^{11}	2.63	65	13	25
PS/PPO 60/40	2700	1.4×10^{10}	2.63	68	20	50

rate dependence of the yield point is captured quite well by a single Eyring process, although the strain softening is slightly under-predicted for large strain rates and slightly over-predicted for low strain rates.

3.1.2. Thermal history

It is well known that physical ageing influences the yield behaviour of glassy polymers. This was first observed by Horsley [40] in 1958 for PVC, and later this was reported for PC [6] and PS [8,41]. Fig. 4 presents the experimental results of compression tests on two PS samples, differing in thermal history.

The yield stress and the amount of strain softening are higher for annealed than for quenched polystyrene, whereas the large strain behaviour remains unchanged. From a true strain of approximately -0.2 the initial difference has vanished and the thermal history does not influence the deformation behaviour anymore. The material is in a so-called rejuvenated state [8]. Since the thermal history influences the yield stress and strain softening, the time constant of the viscosity A, the softening slope h and softening limit D_∞ are adapted. In Table 1 the material parameters for all materials used are given.

3.1.3. Network density

To investigate the influence of network density on crazing behaviour, various PS/PPO samples (0, 20 and 40% PPO) are subjected to indentation experiments. The network density of PS/PPO, a compatible mixture in all ratios, increases with increasing fraction PPO, which enhances the strain hardening contribution at large strains (see Fig. 5).

Along with the ability of the compressible Leonov model to capture the deformation behaviour of the PS/PPO blends (continuous lines), Fig. 5 shows that the yield stress is largely unaffected and the strain softening decreases with increasing PPO fraction. The latter is attributed to the fact that stabilising influence of the strain hardening has a noticeable effect at small strains. In Table 1 the material parameters for PS/PPO blends are also given.

The Poisson ratio ($\nu = 0.37$) is not incorporated in the table as it is assumed to be identical for all materials.

3.2. Indentation experiments

3.2.1. Reference sample

To investigate the reproducibility and accuracy of indentations, a reference sample of annealed polystyrene is indented in a sequence of one hundred indentations. Fig. 6 presents a series of representative indentation curves, differing in maximum load level. The coinciding experimental curves (markers) at distinct maximum load levels illustrate the reproducibility and accuracy of the experiments. The numerical simulation of the indentation process (continuous line) gives a good agreement in the relevant portion. Only a slight adjustment had to be made to the time-constant A to account for the difference in yield stress, due to thermal-history effects, of the indentation and uni-axial compression samples. In the parameter set for annealed polystyrene of Table 1, this was already accounted for.

The force-displacement curves are characteristic for polymer indentation: a monotonic rise of the loading curve and, after a force maximum, an unloading curve with a gradually decaying slope. The area between the loading and the unloading curve represents, besides the work required to deform the material plastically, a time-dependent component. Upon unloading the deformed material will experience relaxation which, dependent on the time-scale of the experiment, will continue after unloading. This time-dependent relaxation behaviour is also responsible for the

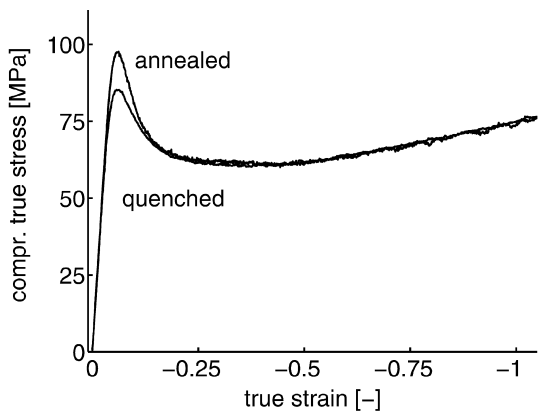

Fig. 4. Influence of thermal history on intrinsic behaviour in compression experiments: annealing results in an increased yield stress and strain softening.

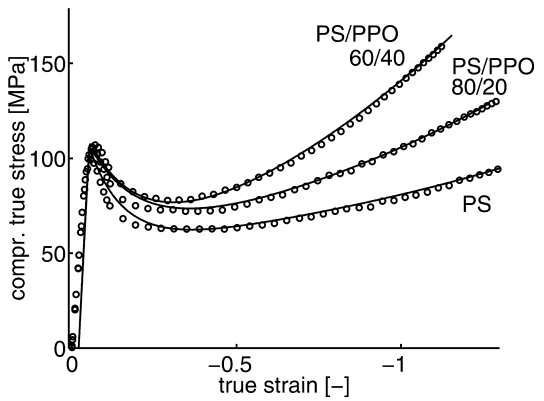

Fig. 5. Compressive behaviour of PS/PPO blends: increased network density results in an enhanced strain hardening contribution.

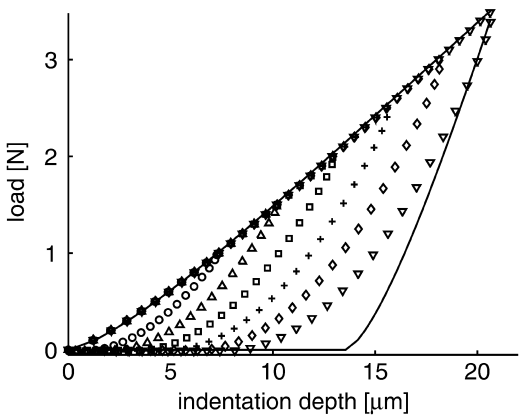

Fig. 6. Experimental force-displacement curves of indentations on PS at various load levels (different markers); the continuous line represents the numerical simulation.

smooth transition from loading to unloading at the load maximum, and the gradual decay of the slope of the unloading curve at low forces.

3.2.2. Loading rate and thermal history

That indentation experiments are sensitive enough to discriminate strain rate and thermal-history effects can be seen in the results shown in Fig. 7. Since the loading curve is predominantly determined by the yield stress and elastic modulus, an increasing strain rate raises the resistance to indentation and results in a steeper loading curve.

Annealing induces a subtle increase in yield stress relative to a quenched sample (see Fig. 4). Since it is known that thermal history has only a slight influence on the elastic modulus [42], the increased resistance to indentation after annealing can be fully attributed to the increased yield stress after annealing.

3.2.3. Network density

The indentations performed on PS/PPO demonstrate the difficulty in discriminating between the contribution of modulus and yield stress on the loading curve. Fig. 5 and the values in Table 1 show that with increasing PPO fraction, the modulus slightly decreases while the yield stress slightly increases. The influence of these counteracting effects is shown in Fig. 8: for PS/PPO with 20% PPO (squares) the resistance to indentation increased relative to pure PS (circles) while for 40% PPO (triangles) and pure PS the loading curves coincide. The remaining plastic indent indicates that there is indeed a difference between PS and PS/PPO with 40% PPO.

3.3. Identification of a craze-nucleation criterion

3.3.1. Reference sample

At high indentation loads crazes are formed, departing from the edge of the contact, between indenter and sample, in radial direction, see Fig. 9b. In situ monitoring of the indentation process showed that these crazes are initiated in the loading stage of the experiment. A sequence of indentation experiments, with a load rate of 0.1 Ns^{-1}, increasing in force (at least 10 indentations at each force step) are performed on the reference sample (annealed PS). At each force step the number of crazes were counted. Fig. 9a shows the number of crazes observed after indentation, at various load levels, as function of the applied load. The markers (circles = annealed PS) represent the average number of crazes observed at a single force step. The continuous line through these average values indicates a

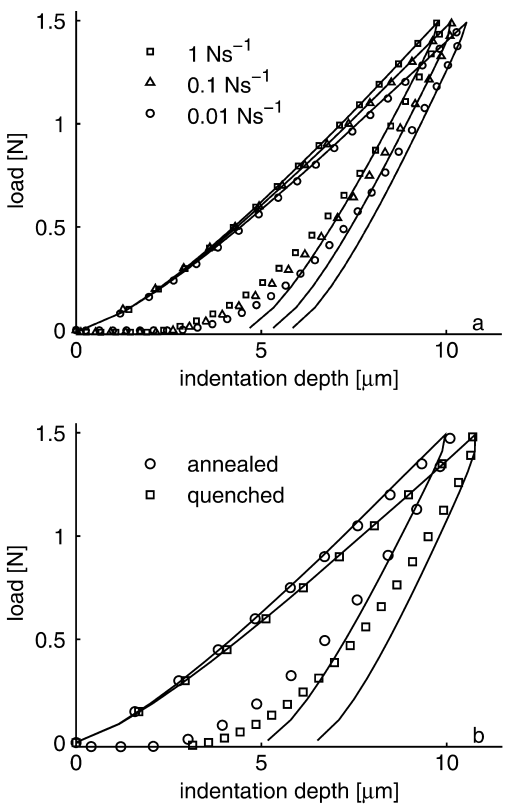

Fig. 7. Influence of strain rate (a) and thermal treatments (b) on the experimental indentation curves (markers) of PS, continuous lines represent numerical simulations.

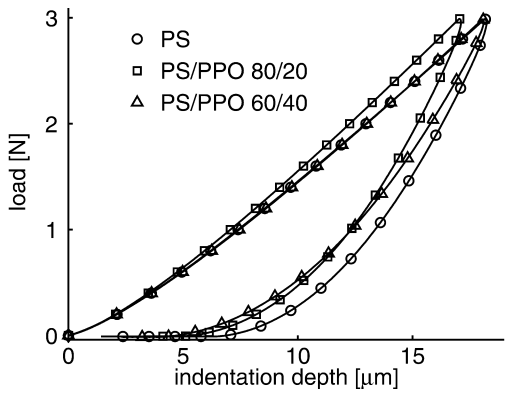

Fig. 8. Experimental force-displacement curves for PS (circles), PS/PPO 80/20 (squares) and PS/PPO 60/40 (triangles), the continuous lines to guide the eye.

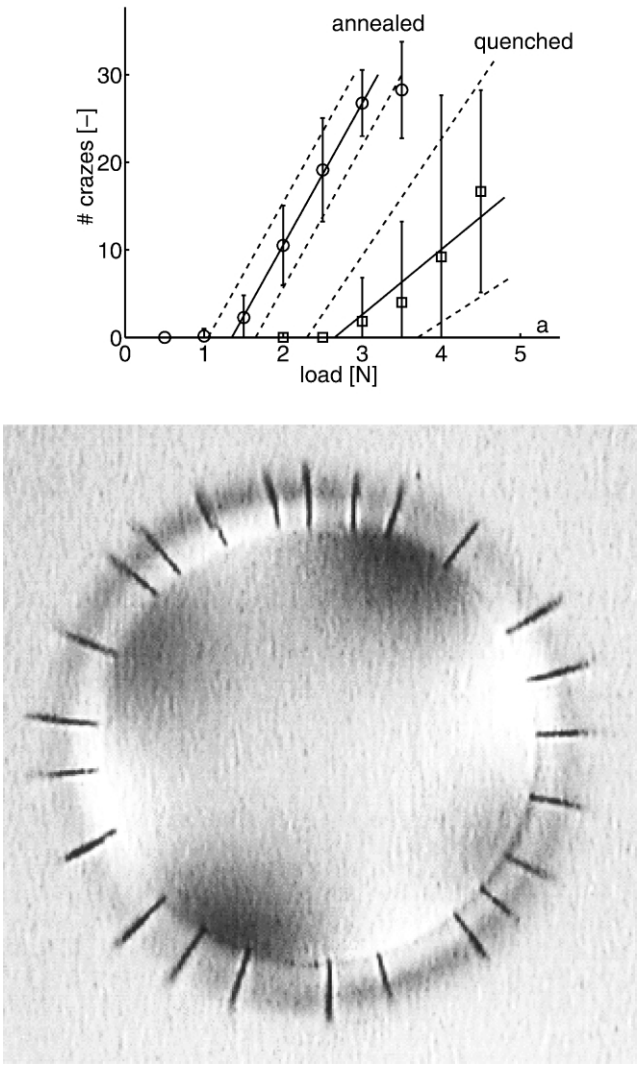

Fig. 9. Number of crazes formed during indentation (a), continuous lines indicate the average values, the dashed lines the 95% confidence interval, for annealed PS (circles) and quenched PS (squares), and a microscopic picture of a plastic indent with crazes (b).

linear increase of the number of crazes with increasing load. Enveloping the continuous lines a probability corridor (dashed lines) is drawn which accounts for the distribution (95% confidence interval) on the number of crazes observed.

Extrapolation of the line to the x-axis marks the onset of craze-initiation. It is concluded that an average force of 1.35 N is required to initiate crazing during indentation of annealed PS. Considering the distribution in the observations, a craze-initiation force-interval of 1.05–1.65 N is assumed.

Since the crazes are initiated during the loading part and the loading part was adequately described (see Figs. 6 and 7), finite element simulations are used to investigate the stress distribution around the indenter at the initiation of crazes. These simulations show that during indentation the material adjacent to the indenter is pushed outwards in radial direction, and hence induce positive stresses in circumferential direction. In Fig. 10, the hydrostatic stress in plotted in the region of interest, near the contact of indenter and sample, where the crazes are observed experimentally. A maximum in hydrostatic stress is found in this region, near the surface of the sample. The requirement that crazing is preceded by plastic deformation is met, as the softening variable D is larger than 0 in this region, this implies that the material is plastically deformed.

Fig. 11 shows the maximum hydrostatic stress as function of load. While the load is raised with a load rate identical to the experiments, from 0 to 4 N, the hydrostatic stress level increases. The position at which this maximum occurs shifts as the contact circle of indenter and sample moves in radial direction with increasing load. This results in a staggered path of maximum hydrostatic stress, shown in Fig. 11.

From the average force required for craze initiation, as derived from Fig. 9 and considering the experimental error on craze-observation, the critical hydsrostatic stress for craze nucleation is 40($\pm$2) MPa.

3.3.2. Thermal history

To validate the conclusion that a craze initiation criterion, composed of the requirement of a localised plastic zone and a critical hydrostatic stress, required for void nucleation, is appropriate to describe void nucleation, the influence of thermal history is investigated. The previous results for annealed PS are therefore compared to craze-initiation in a quenched PS sample. The material parameters for quenched PS are also presented in Table 1. Figs. 4 and 7b already showed that the yield stress and the resistance to indentation for quenched PS are lower than for annealed PS. Microscopic observations reveal that the crazes formed in quenched PS are not only much smaller and thinner compared to annealed PS, they are also more difficult to detect and can only be visualised using polarised light. Besides the force required to initiate crazes (2.6 N), the distribution in values of the number of crazes observed in quenched PS is much larger (ranging from 2.3 to 3.7 N), see Fig. 9.

The maximum hydrostatic stress as function of the applied load is also shown for the quenched sample (squares) in Fig. 11. The slope of the maximum hydrostatic

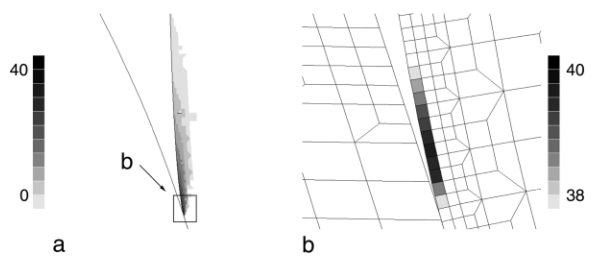

Fig. 10. Numerical prediction of the build-up of hydrostatic stress in the region where crazes are observed experimentally (a), zoomed in on the area of interest (b).

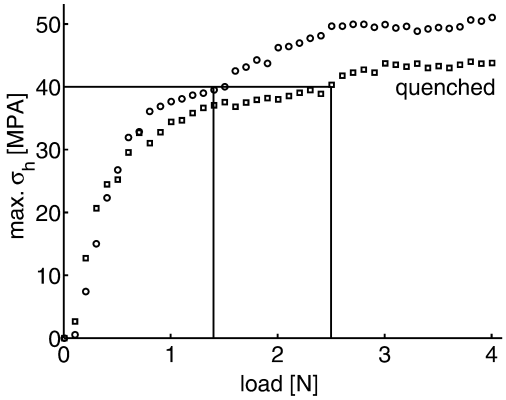

Fig. 11. Maximum hydrostatic stresses in simulation; average critical force and corresponding critical hydrostatic stress for annealed PS (circles) and quenched PS (squares).

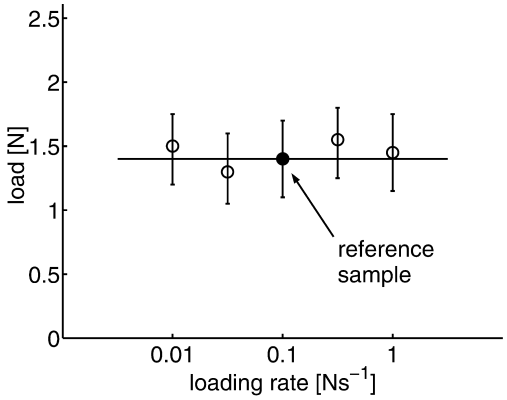

Fig. 12. The critical load at which crazes are first observed in PS is not influenced by the loading rate.

stress versus load are comparable for the annealed and the quenched sample up to 0.7 N. At a hydrostatic stress approximately 30 MPa, the paths begin to diverge as the hydrostatic stress in the quenched sample evolves slower. The critical hydrostatic stress of 40 MPa, determined for annealed PS, corresponds to a critical force of craze formation in the quenched material of 2.5 N. Considering the experimentally observed 2.6 N (within a range of 2.3–3.7 N), it is reasonable to assume that the hydrostatic stress required for void-nucleation both annealed and quenched polystyrene equals 40 MPa.

3.3.3. Loading rate

Further validation of this craze-initiation criterion is done by investigating the influence of the loading rate during indentation. The stress-strain behaviour and the indentation curves of PS are dependent on the loading rate, as was shown in Figs. 3 and 7a. Again the reference sample of annealed PS and its material parameters (see Table 1) are used in these experiments and simulations. For indentations 5 loading rates are taken, ranging from 0.01 to 1 Ns^{-1}.

With increasing loading rate, the resistance to indentation rises, as was shown in Fig. 7a. Besides the increase in yield stress at increasing loading rate, visco-elastic effects can also play a role as the time scale of the experiments shortens.

Fig. 12 shows the force-interval at which crazes in the experiment are observed for all different loading rates applied. The procedure to determine these intervals was identical to the procedure used for the annealed and quenched PS (see Fig. 9). The force-intervals, at which crazing is observed experimentally, prove to be nearly independent of the loading rate within the range measured.

Numerical simulations were performed at the same loading rates and the results are presented in Fig. 13. The slight differences seen in the indentation curves (Fig. 7a) have virtually no influence on the development of the maximum hydrostatic stress. Since the force interval at which crazes are observed is similar at all loading rates, it can be concluded that the critical hydrostatic stress at which crazes are initiated is independent of the loading rate. This is consistent with the findings of work by Tervoort [43].

3.3.4. Network density

In the previous sections a void-nucleation criterion was identified for polystyrene, based on the assumption that void-nucleation is preceded by localised plastic deformation and incipient void nucleation by dilative stresses. This critical hydrostatic stress of 40 MPa proved to be independent of the thermal history and strain rate. Among others, Kramer and co-workers [3,44] and Wu [45] suggested that the network density influences the crazing behaviour and critical craze-nucleation stress. Therefore, the procedure followed to determine a critical craze-nucleation stress for polystyrene is repeated for PS/PPO blends. The network density of polystyrene increases when blended with PPO. The material parameters used in the simulations are given in Table 1. In Figs. 5 and 8 it was shown that for an increasing PPO fraction the yield stress slightly increases, the modulus decreases but above all, the strain hardening contribution is strongly enhanced.

Fig. 14 shows the number of crazes formed during indentation at various load levels. The force required to initiate crazes increases with PPO fraction and thus with the

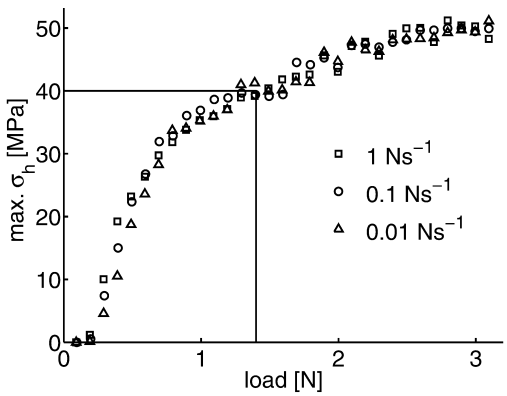

Fig. 13. Building up of hydrostatic stress during loading at various loading rates for annealed PS: no rate dependence.

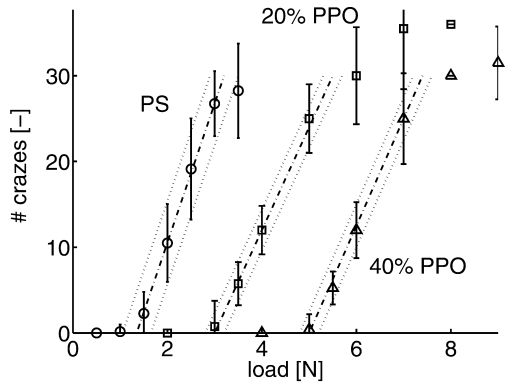

Fig. 14. Number of crazes formed by indentation for annealed PS (circles), PS/PPO 80/20 (squares) and PS/PPO 60/40 (triangles). The broken lines represent the 95% confidence interval.

network density. For the blend with 20% PPO (squares) the force is 3(±0.2 N), for 40% PPO (triangles) this is 5(±0.2 N).

Simulations of these indentation experiments, in which the maximum hydrostatic stress is again monitored, show that despite the differences in the indentation curves (see Fig. 8), the development of the maximum hydrostatic stress in the sample is barely influenced, see Fig. 15.

All curves have a positive slope with an increasing indentation force. The critical force for pure PS is reached at 1.35 N (as shown before), which corresponds to a critical hydrostatic stress of approximately 40 MPa. According to the experiments crazing is observed at a force of 3.0 N for PS/PPO with 20% PPO, corresponding to a hydrostatic stress of 50 MPa (dotted lines in Fig. 16) and for a fraction of 40% PPO the critical indentation force is 5.1 N, corresponding to a hydrostatic stress of approximately 55 MPa. The uncertainty intervals around the critical forces and hydrostatic stress are similar for all materials. The network density for PS and PS/PPO blends, is obtained by DMTA [14,46]. For PS a network density of 3.0×10^{25} chains m^{-3} is found. With increasing PPO fraction the network density rises to 4.9×10^{25} chains m^{-3} (20% PPO) and 7.9×10^{25} chains m^{-3} (40% PPO). In Fig. 16 the

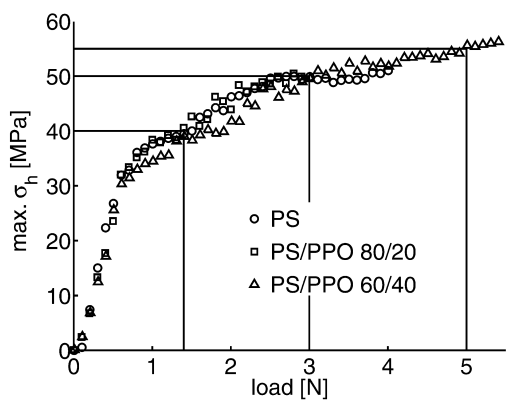

Fig. 15. Development of σ_h as function of load for annealed PS (circles), PS/PPO 80/20 (squares) and PS/PPO 60/40 (triangles).

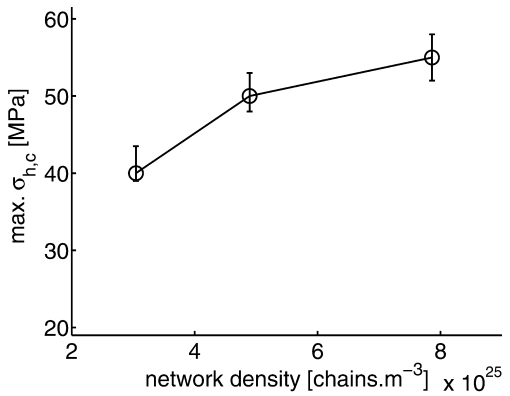

Fig. 16. Critical hydrostatic stress as a function of the network density.

critical hydrostatic stress is given as function of network density.

It can be concluded that the resistance to craze-nucleation of glassy polymers, like PS and PS/PPO, increases with increasing network density, which is in full agreement with the findings of Sauer [47]. The extrapolation of the trend in Fig. 16 to higher network densities, e.g. polycarbonate, gives a good approximation of the critical craze nucleation stress reported by Narisawa and co-workers ($\nu_e = 3.0 \times 10^{26}$ chains m^{-3} [45], $\sigma_{h,c} = 90$ MPa [31]). However, it must be noted that with increasing PPO in the PS/PPO blends also the glass transition temperature of these materials increases. This of course alters the molecular mobility of the materials, an effect that is not considered within the scope of this work. A series of experiments at various temperatures could reveal the importance of this parameter.

4. Conclusions

A combination of a numerical analysis using a proper constitutive model that can cover the rate dependent intrinsic yield behaviour, and a local, rate independent, craze-nucleation criterion can be used effectively to predict craze initiation in glassy polymers.

Micro-indentation of polystyrene at a sufficiently high load leads to crazing. Using the numerical model, the hypothesis of Kramer [2] is confirmed that crazing of polymers is preceded by localised plastic deformation. Due to the non-linear nature of yielding, strain softening results in localisation of deformation as the plastic strain increases, accompanied by a build-up of hydrostatic stress. The hydrostatic stress is the only parameter that initiates void-nucleation after the material shows local deformation and softening.

During the loading stage of indentation crazes are formed, beginning near the contact circle between indenter and specimen in radial direction. Visualisations, by means of microscopy, enable determination of the number of crazes and the critical force at which they are formed.

From the numerical simulations the critical hydrostatic stress for void nucleation is determined to be 40 MPa for annealed PS, and this event occurs just outside the contact zone between polystyrene and indenter. This criterion is validated by varying thermal history and loading rate during indentation. Quenched PS shows very tiny crazes at a higher force, the trend depicted by the numerical simulation is good and the prediction by the craze-nucleation criterion agrees with the observations. The exact value of the crazing force for the quenched sample is difficult to predict. Varying the loading rate does not influence the crazing force and both the numerical model and experiments resulted in the same force. The post-yield behaviour was altered by adding PPO to PS, due to which the network density increased. An increase of the network density results in a higher value of the critical craze-nucleation stress, 50 MPa for the blend with 20% PPO and 55 MPa for the blend with 40% PPO. Although this indicates a crucial role of the network density on the process of craze nucleation, other parameters such as molecular mobility, which vary for the different blends, have not been explored and can be subject of investigation in future work.

Acknowledgements

The authors wish to acknowledge the financial support provided by the Dutch Technology Foundation (STW) (Grant EWT.3766).

Appendix A

In this appendix the relevant equations of the compressible Leonov model are summarised. An elaborate description of this elasto-visco plastic model can be found in Govaert et al. [11] and Tervoort et al. [24,25].

$$\boldsymbol{\sigma} = \mathbf{s} + \mathbf{r} \tag{1}$$

$$\mathbf{s}^d = G\tilde{\mathbf{B}}_e^d \quad \text{and} \quad \mathbf{s}^h = \kappa(J-1)\mathbf{I} \tag{2}$$

$$\dot{J} = J\cdot\mathrm{tr}(\mathbf{D}) \tag{3}$$

$$\tilde{\mathbf{B}}_e = (\mathbf{D}^d - \mathbf{D}_p)\cdot\tilde{\mathbf{B}}_e + \tilde{\mathbf{B}}_e\cdot(\mathbf{D}^d - \mathbf{D}_p) \tag{4}$$

$$\mathbf{r} = G_R\tilde{\mathbf{B}}^d \tag{5}$$

$$\mathbf{D}_p = \frac{\mathbf{s}^d}{2\eta(\tau_{eq}, D, p)} \tag{6}$$

$$\eta(\tau_{eq}, D, p) = A(D,p)\tau_0 \frac{\frac{\tau_{eq}}{\tau_0}}{\sinh\left(\frac{\tau_{eq}}{\tau_0}\right)} \tag{7}$$

$$\tau_{eq} = \sqrt{\frac{1}{2}\mathrm{tr}(\mathbf{s}^d\cdot\mathbf{s}^d)} \tag{8}$$

$$\dot{D} = \mathrm{h}\left(1 - \frac{D}{D_\infty}\right)\dot{\gamma}_p \tag{9}$$

$$\dot{\gamma}_p = \sqrt{2\mathrm{tr}(\mathbf{D}_p\cdot\mathbf{D}_p)}$$

References

[1] Kambour RP. J Polym Sci: Macromol Rev 1973;7:1–154.
[2] Kramer EJ. Microscopic and molecular fundamentals of crazing. In: Kausch HH, editor. Crazing in polymers. Advances in polymer science 91/92, Berlin: Springer; 1983. p. 1–56.
[3] Kramer EJ, Berger LL. Craze growth and fracture. In: Kausch HH, editor. Crazing in polymers. Advances in polymer science 91/92, vol. 2. Berlin: Springer; 1990. p. 1–68.
[4] Kinloch AJ, Young RJ. Fracture behaviour of polymers, 2nd ed. Amsterdam: Applied Science Publishers; 1985.
[5] Argon AS, Hannoosch JG. Philos Mag 1977;36(5):1195–216.
[6] Adam GA, Cross A, Haward RN. J Mater Sci 1975;10(9):1582–90.
[7] Cross A, Haward RN, Mills NJ. Polymer 1979;20(3):288–94.
[8] Hasan OA, Boyce MC. Polymer 1993;34(24):5085–92.
[9] Bauwens JC. J Mater Sci 1978;13(7):1443–8.
[10] G'Sell C. Plastic deformation of glassy polymers: constitutive equations and macromolecular mechanisms. In: McQueen H, editor. Strength of metals and alloys. Oxford: Pergamon Press; 1986. p. 1943–82.
[11] Govaert LE, Timmermans PHM, Brekelmans WAM. J Engng Mater Technol 2000;122(2):177–85.
[12] Tervoort TA, Govaert LE. J Rheol 2000;44(6):1263–77.
[13] Govaert LE, van Melick HGH, Meijer HEH. Polymer 2001;42(3): 1271–4.
[14] van Melick HGH, Govaert LE, Meijer HEH. On the origin of strain hardening in glassy polymers, in press.
[15] van Melick HGH, Govaert LE, Meijer HEH. Localisation phenomena in glassy polymers: Influence of thermal and mechanical history, in press.
[16] Ender DH, Andrews RD. J Appl Phys 1965;36(10):3057–62.
[17] Henkee CS, Kramer EJ. J Polym Sci 1984;22(4):721–37. Polymer Physics Edition.
[18] Boyce MC, Parks DM, Argon AS. Mech Mater 1988;7(1):15–33.
[19] Hasan OA, Boyce MC, Li XS, Berko S. J Polym Sci, Part B: Polym Phys 1993;31(2):185–97.
[20] Arruda EM, Boyce MC. Int J Plast 1993;9(6):697–720.
[21] Boyce MC, Arruda EM, Jayachandran R. Polym Engng Sci 1994; 34(9):716–25.
[22] Wu PD, van der Giessen E. J Mech Phys Solids 1993;41(3):427–56.
[23] Wu PD, van der Giessen E. Int J Plast 1995;11(3):211–35.
[24] Tervoort TA, Smit RJM, Brekelmans WAM, Govaert LE. Mech Time-dependent Mater 1998;1(3):269–91.
[25] Tervoort TA, Klompen ETJ, Govaert LE. J Rheol 1996;40(5): 779–97.
[26] Smit RJM, Brekelmans WAM, Meijer HEH. Comput Meth Appl Mech Engng 1998;155(1-2):181–92.
[27] Smit RJM, Brekelmans WAM, Meijer HEH. J Mech Phys Solids 1999;47(2):201–21.
[28] Smit RJM, Brekelmans WAM, Meijer HEH. J Mater Sci 2000;35(11): 2855–67.
[29] Smit RJM, Brekelmans WAM, Meijer HEH. J Mater Sci 2000;35(11): 2869–79.
[30] Smit RJM, Brekelmans WAM, Meijer HEH. J Mater Sci 2000;35(11): 2881–92.
[31] Ishikawa M, Narisawa I, Ogawa H. J Polym Sci 1977;15(10): 1791–804. Polymer Physics Edition.
[32] Narisawa I, Ishikawa M, Ogawa H. Philos Mag A 1980;41(3): 331–51.
[33] Ishikawa M, Ogawa H, Narisawa I. J Macromol Sci, Part B: Phys 1981;B19(3):421–43.

[34] Camwell L, Hull D. Philos Mag 1973;27(5):1135–50.
[35] Kells D, Mills NJ. Philos Mag A 1981;44(5):1149–63.
[36] van Melick HGH. Internal report, Materials Technology, Eindhoven University of Technology; 2001.
[37] van Melick HGH, van Dijken AR, den Toonder JMJ, Govaert LE, Meijer HEH. Philos Mag A 2002;82(10):2093–102.
[38] Simmons G, Wang H. Single crystal elastic constants and calculated aggregate properties: A handbook, 2nd ed. Cambridge: MIT Press; 1971.
[39] van Krevelen W. Properties of polymers. Amsterdam: Elsevier; 1972.
[40] Horsley RA. The properties of lightly plasticized PVC compounds. In: Morgan P, editor. Plastics progress. London: Iliffe and Sons; 1958.
[41] Marshall AS, Petrie SEB. J Appl Phys 1975;46(10):4223–30.
[42] Hutchinson JM. Prog Polym Sci 1995;20(4):703–60.
[43] Tervoort TA. PhD thesis, Eindhoven University of Technology 1996; Chapter 4. http://alexandria.tue.nl/extra3/proefschrift/PRF11B/9601397.pdf.
[44] Donald AM, Kramer EJ. J Mater Sci 1982;17(7):1871–9.
[45] Wu S. Polym Engng Sci 1990;30(13):753–61.
[46] Prest jr WM, Porter RS. J Polym Sci, Part A2: Polym Phys 1972; 10(9):1639–55.
[47] Sauer JA, Hara M. Crazing and fatigue of polymers. In: Kausch HH, editor. Crazing in polymers. Advances in polymer science 91/92, vol. 2. Berlin: Springer; 1990. p. 69–118.